SCIENTIFIC REPORTS

OPEN

Polarized Raman scattering study of kesterite type Cu_2ZnSnS_4 single crystals

Received: 22 September 2015
Accepted: 10 December 2015
Published: 18 January 2016

Maxim Guc[1,4], Sergiu Levcenko[2], Ivan V. Bodnar[3], Victor Izquierdo-Roca[4], Xavier Fontane[4], Larisa V. Volkova[3], Ernest Arushanov[1] & Alejandro Pérez-Rodríguez[4,5]

A non-destructive Raman spectroscopy has been widely used as a complimentary method to X-ray diffraction characterization of Cu_2ZnSnS_4 (CZTS) thin films, yet our knowledge of the Raman active fundamental modes in this material is far from complete. Focusing on polarized Raman spectroscopy provides important information about the relationship between Raman modes and CZTS crystal structure. In this framework the zone–center optical phonons of CZTS, which is most usually examined in active layers of the CZTS based solar cells, are studied by polarized resonant and non-resonant Raman spectroscopy in the range from 60 to 500 cm^{-1} on an oriented single crystal. The phonon mode symmetry of 20 modes from the 27 possible vibrational modes of the kesterite structure is experimentally determined. From in-plane angular dependences of the phonon modes intensities Raman tensor elements are also derived. Whereas a strong intensity enhancement of the polar E and B symmetry modes is induced under resonance conditions, no mode intensity dependence on the incident and scattered light polarization configurations was found in these conditions. Finally, Lyddane-Sachs-Teller relations are applied to estimate the ratios of the static to high-frequency optic dielectric constants parallel and perpendicular to *c*-optical axis.

The Cu_2ZnSnS_4 (CZTS) quaternary compound is widely discussed over the last few years as an active layer in thin films photovoltaic devices[1–11]. Although the electronic properties of the CZTS-heterojunction solar cells have been studied extensively the knowledge of the CZTS basic properties is still limited. Particularly, the crystal structure[4,12], intrinsic optoelectronic[5,6,8,9,13–15] and electrical properties[9,10,16,17] are not well understood. The development of photovoltaic technologies based on this semiconductor strongly requires for the availability of experimental techniques suitable for the analysis of the crystalline quality of the CZTS absorbers. Recently, Raman spectroscopy (which is a nondestructive optical technique) has showed a high potential to be used for characterization of the structure disorder[18–20], secondary phases[21,22], stress, compositional effects and phonon confinement effects in CZTS semiconductor[23].

In 1991 Himmrich and Haeuseler first reported characteristic Raman peaks at 285, 336 and 362 cm^{-1} for CZTS powdered samples[24]. Since then several of papers with CZTS lattice vibration spectra have been published, but in most of these reports Raman spectroscopy serves for samples characterization and establishing link between process parameters and films growth[21,22]. A more quantitative Raman analysis can be found only in few reports[23,25], which include a very detailed analysis of the vibrational properties of CZTS from the simultaneous fitting of the Raman spectra performed with six different excitation wavelengths on device grade polycrystalline layers[25]. In this work, a first assignment of the symmetry of the modes is made, based in the comparison with theoretical calculations reported in the literature and with polarization measurements, and the presence of phonon confinement effects characteristic of nano-crystalline layers or related to the presence of structural defects has also been analysed in[23]. As reported in this work, these effects determine a broadening and a shift to lower frequencies of the main Raman peaks, and take place for samples with crystal sizes lower than 50 nm.

However, polarization measurements performed on polycrystalline layers have limitations for the assignment of the symmetry of Raman peaks, because of the randomly oriented grains in the layers. Unambiguous

[1]Institute of Applied Physics, Academy of Sciences of Moldova, Chisinau, MD 2028, Moldova. [2]Helmholtz Zentrum Berlin fur Materialien und Energie, Berlin, D-14109, Germany. [3]Department of Chemistry, Belarusian State University of Informatics and Radioelectronics, Minsk, Belarus. [4]IREC, Catalonia Institute for Energy Research, Sant Adrià del Besòs (Barcelona), 08930, Spain. [5]IN2UB, Departament d'Electrònica, Universitat de Barcelona, Barcelona, 08028, Spain. Correspondence and requests for materials should be addressed to M.G. (email: mguc@irec.cat)

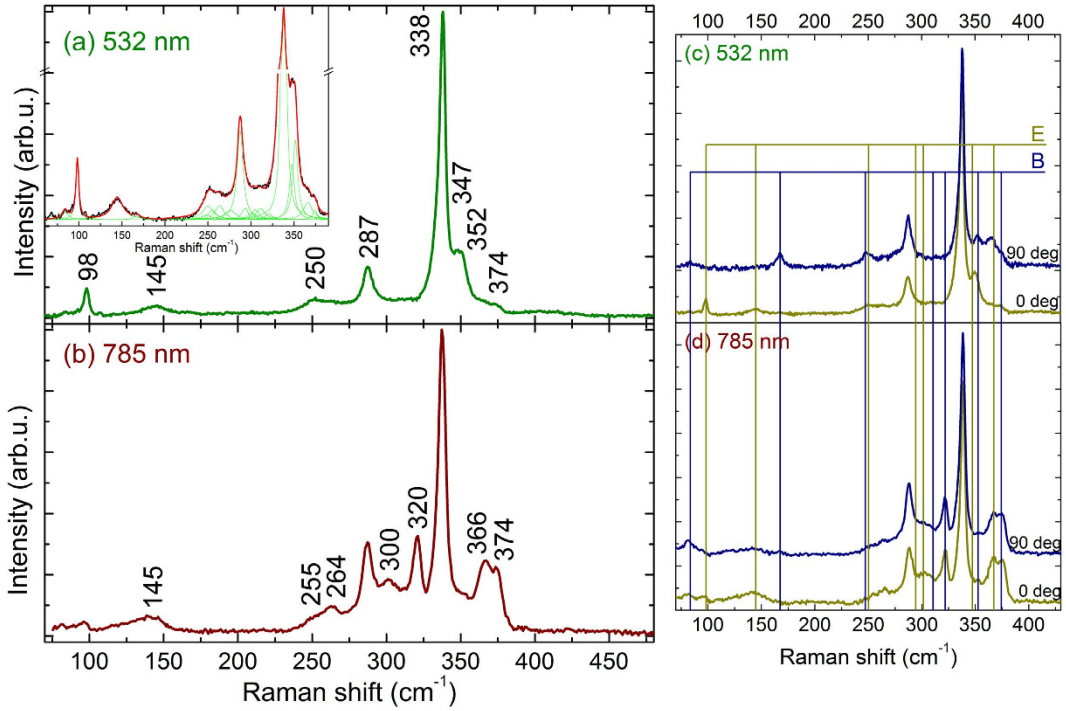

Figure 1. Raman spectra of Cu_2ZnSnS_4 single crystals excited with laser line 532 nm (a) and 785 nm (b), close to resonant conditions. Inset of figure (**a**) shows the fitting (red curve) of the experimental Raman spectra (black curve) with Lorentzian curves (green). Here the breaks on intensity scales were performed to show weaker peaks with lower intensity. Figures (**c**,**d**) represent the spectra measured at different polarization configurations. Here angles 0 deg and 90 deg correspond to $<\overline{X}|YY|X>$ and $<\overline{X}|ZZ|X>$ configurations, respectively.

determination of the symmetry and selection rules requires the use of single crystal samples with well-known crystalline orientation. Recent Raman scattering experiments on CZTS single crystals have provided clear evidence for a strong polarization dependence of the Raman peaks on the crystallographic directions of the investigated crystal[26]. However, the valuable information on the Raman tensor elements is not given and phonon modes below 140 cm^{-1} are not studied in this publication.

Here we present the polarized Raman measurements under non-resonant and resonant conditions on oriented CZTS single crystal in the range of 60–500 cm^{-1}. The analysis of Raman mode intensities as a function of in plane angle of the (1 1 2)-plane allows us to determine the symmetry of the phonon modes. As a result the identification of 20 from the 27 possible modes of the kesterite structure is performed, completing the previous identification that was reported in[25,26], and the ratios of Raman tensor elements are evaluated for many of them.

Results and Discussions

The CZTS compound crystallizes in the kesterite type structure, space group $I\overline{4}$. For this space group, taking into account the eight atoms site position in the CZTS unit cell, the group theory[27] yields the following irreducible representation of the twenty four phonons at the center of the Brillouin zone, Γ point (see Supplementary information)

$$\Gamma = 3A \oplus 7B \oplus 7E. \quad (1)$$

Here $3A \oplus 6B \oplus 6E$ modes are Raman active, from them $6B \oplus 6E$ modes are also IR-active, which leads to their LO-TO splitting. E modes are also double degenerated. The rest $B \oplus E$ modes are acoustic. The intensity of a Raman mode depends on the polarizations of the incident and scattered light and the Raman tensor elements for the crystal plane on which measurements are performed (see Supplementary information). It is also possible to distinguish between the B and E symmetry modes by carrying out backscattering measurements on (1 1 2) crystal facet as it has been recently shown for the close related kesterite $Cu_2ZnSnSe_4$ (CZTSe)[28]. The non-polarized Raman spectrum of CZTS single crystal is presented in Fig. 1 (a). Most intense peaks are in accordance with data from previously reported studies on single crystals[26], thin films[21,22,25] and powder samples[18,24,29]. It should be noted, that the number of the experimental modes in the region 220–330 cm^{-1} are less than the theoretically predicted: two A modes, two polar B (TO/LO) modes and two polar E (TO/LO) modes for the kesterite type structure[30–32]. The small Raman cross section of the missing Raman lines and possible overlapping in the position of the peaks might be reasons, why these modes are not clearly seen in the spectra. To resolve this issue we have made resonance Raman scattering measurements using excitation photons with energy close to the band gap transition in CZTS. In these conditions, an enhancement in the intensity of some of the polar modes is

A		*a/b*	B (TO+LO)		*c/d*	E (TO+LO)		*e/f*
Theor	Exper	||/⊥	Theor	Exper	||/⊥	Theor	Exper	||/⊥
270.0	276	—	87.8 + 88.2	**84**	<0.1/0.13 ± 0.09	82.2 + 82.2	**83**	0.97 ± 0.09/0.85 ± 0.15
281.7	**287**	1.28 ± 0.07/—	99.3 + 99.3	—	—	102.9 + 103.0	**98**	0.92 ± 0.03/1.10 ± 0.05
338.5	**338**	0.93 ± 0.04/—	168.2 + 169.5	**167**	<0.1	150.0 + 150.5	**145**	0.92 ± 0.06/1.12 ± 0.06
			237.9 + 253.7	**248** + 255	<0.1	247.8 + 254.8	250/*264*	—
			307.6 + 311.4	*311* + *320*	—	278.0 + 290.3	*293*/*300*	—
			357.0 + 373.6	**352** + *374*	<0.1	351.1 + 365.3	**347**/*366*	0.89 ± 0.05/0.85 ± 0.07

Table 1. Symmetry of the Raman peaks of Cu_2ZnSnS_4 kesterite type quaternary compound and ratios of Raman tensor elements. Peaks position indicated in italic correspond to peaks where a tentative symmetry assignment is proposed based on comparison with theoretical calculations[32]. For peaks position indicated in bold the ratio of Raman tensor elements was calculated.

expected[33–36]. The non-polarized resonant Raman spectrum of CZTS single crystal is shown in Fig. 1(b). New peaks at 255, 264, 300, 320 and 366 cm^{-1} are clearly identified in the spectrum. In addition, there is also a strong increase in the intensity of the peak at 374 cm^{-1}. We assume that these peaks are LO components of the polar B and E symmetry modes, which gain their intensity due to Fröhlich electron-phonon interaction[33]. Raman spectra were fitted with Lorentzian functions (an example of such decomposition is presented in the inset of Fig. 1 (a)) based on the phonon modes positions found under resonance and non-resonance conditions. The full width at the half maximum (FWHM) of the most intense peaks was in the range 5–8 cm^{-1}, which confirms the good crystallinity of the grown samples. In the 230–300 cm^{-1} spectral region, some phonon modes have larger FWHM values (10–15 cm^{-1}), which might be due to the presence of the additional multiphonon peaks[37]. It is interesting to remark that weaker peaks at 643 and 740 cm^{-1} (not shown here) have also been detected. These peaks match well with the second order of the resonant enhanced modes at 320 and 374 cm^{-1}, respectively. Recently high overtones phonon modes were also found for CZTS crystals at 664, 968 and 1323 cm^{-1} [38].

The Raman spectra measured with $<\overline{X}|YY|X>$ and $<\overline{X}|ZZ|X>$ polarization configurations, according to Porto notations[39], are plotted in Fig. 1(c,d). The two most intense peaks at 287 and 338 cm^{-1} are clearly identified with the dominant non-polar A-symmetry modes. Based on the selection rules (see Supplementary Table S3) for non-resonance condition Raman peaks at 84, 167, 248 and 352 cm^{-1} visible in the $<\overline{X}|YY|X>$ spectra are attributed to B-symmetry modes, while those peaks at 83, 98, 145 and 347 cm^{-1} visible in the $<\overline{X}|ZZ|X>$ spectra are identified with E-symmetry modes. However, under resonant excitation conditions all Raman peaks maintain near the same intensity in both $<\overline{X}|YY|X>$ and $<\overline{X}|ZZ|X>$ configurations (Fig. 1(d)). These data show a violation under resonant conditions of the selection rules for the polar B and E symmetry modes. For close related $Cu(In,Ga)S_2$ chalcogenides it was found similarity in selection rules for resonant Raman scattering and optical transitions near band edge[40,41]. Thus we may assume that the absence of the polarization behavior in CZTS resonant Raman spectra is due to a small anisotropy of the optical transitions relative to the crystal axis ***c*** as the incoming photon with **Y** polarization is perpendicular to ***c***, while the incoming photon with **Z** polarization has an angle of 35° with the ***c*** axis. By decomposition of Raman spectra with the Lorentzian curves the phonon frequencies of the different modes are obtained and are summarized in Table 1. Here the theoretical results published in ref. 32 are also given and the symmetry of modes indicated in italic is proposed based on this work. It should be noted that position of LO modes was determined from the resonant Raman (RR) spectra, while TO modes were identified based on theoretical calculations[30–32]. As shown, the TO-LO splitting does not exceed 16 cm^{-1} even for the modes with highest wavenumber. Thus in the fitting of the spectra we added the peaks of the TO components close to the LO ones until the quality of the fitting was not improved. However, the estimated position of the TO components can have an uncertainty in the range of 1–2 cm^{-1}.

The identification of the exact position of a third A symmetry mode in the region 220–330 cm^{-1} was more complex from the analysis of our measurements. Dimitrievska *et al.*[25] identified this mode with a peak located at 306 cm^{-1} that appears mainly when measuring with 633 nm and 785 nm excitation wavelengths, and this identification was proposed mainly from comparison with the theoretical data reported in ref. 30. However, the analysis of the spectra measured on the single crystal samples has not allowed to corroborate this identification. On the other hand, the detailed fitting of the experimental polarization spectra measured with different angles on the (1 1 2) crystal plane suggests the presence of a contribution at 276 cm^{-1} with A symmetry. The assignment of this contribution with the third A symmetry mode of the kesterite structure agrees with the fact that the theoretical calculations in ref. 32 predict two A modes relatively close (at 270.0 cm^{-1} and 281.7 cm^{-1}) and a mode that is more separated at higher frequencies (at 338.5 cm^{-1}, corresponding to the dominant mode in the spectra). Similar results were predicted from other theoretical calculations[31]. This also agrees with the experimental identification in the close related CZTSe kesterite, where two close spaced A-modes at lower frequencies were found[28].

The accurate analysis of the polarized Raman spectra measured at different angles θ on the (1 1 2) plane has allowed to corroborate the symmetry assignment of several of the vibrational modes. Fitting of the intensity of the peaks as a function of the in plane angle θ, following the equations derived in ref. 28 (see the Supplementary Table S3) for the single crystal CZTSe kesterite with the similar crystalline orientation has allowed also to make an estimation of the ratios of the Raman tensor elements as indicated in Table 1. Examples of angular dependencies obtained for modes with different symmetry are exhibited in Fig. 2, where the solid lines correspond to the fitting of the experimental data with the equations derived in ref. 28. Here we see that in case of the A symmetry

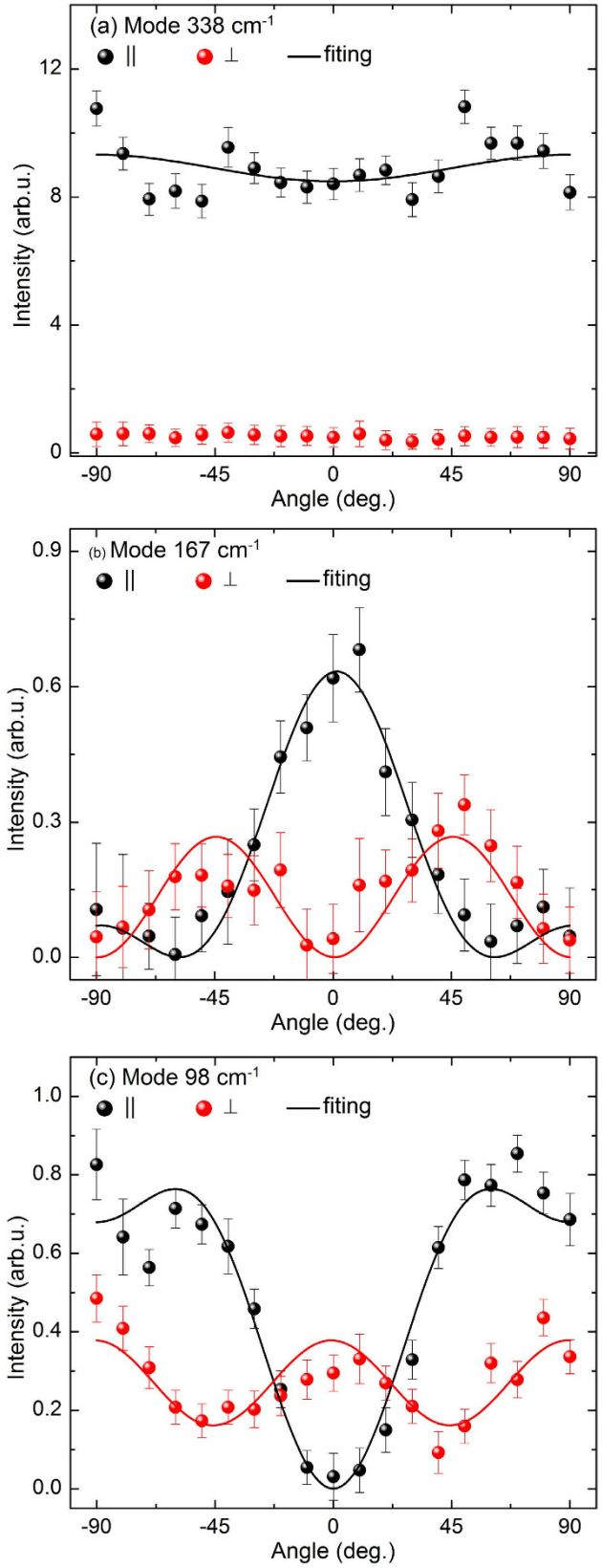

Figure 2. Examples of the angular dependence of the Raman peaks intensities of the A (a), B (**b**) and E (**c**) mode symmetry. Solid lines are fitting to corresponding Eqs. from Supplementary Table S3 for parallel and perpendicular configurations.

modes their intensity is almost independent on the rotation angle in parallel configuration and is close to zero in perpendicular configuration (Fig. 2(a)). Similar results are found in case of other kesterite type compounds as CZTSe and $Cu_2ZnGeSe_4$[28] and can be explained by the close values of *a* and *b* tensor elements, i.e. $a/b \approx 1$. The fitting of angular dependence of some B and E symmetry modes was also performed (see examples at Fig. 2 (b,c)). For these modes the obtained results are also similar to those previously reported for the kesterite CZTSe and $Cu_2ZnGeSe_4$ compounds[28], with a strong anisotropy for the tensor elements of B symmetry modes and a much smaller anisotropy for tensor elements of E symmetry modes. This appears as a characteristic property of kesterite type quaternary compounds. Since the properties of the phonons are directly related with Raman tensor elements, the estimated ratio of the tensor elements could be useful for the prediction of the mode intensities or angular intensity patterns for others crystal geometries. For instance, Raman measurements on (0 0 1)-plane with parallel geometry (incident and scattered light polarization either along [1 0 0] or [0 1 0]) should result in very low B-mode intensities in comparison to the cross geometry-case due to large anisotropy for B-mode tensor elements. Indeed the latter B-mode behavior was observed in polarization resolved experiment in ref. 26, while no explanation was given.

Finally, the analysis of the frequencies of the polar modes has allowed us to estimate the ratio of the static (ε_0) to optic (ε_∞) dielectric constants. This is based on the Lyddane-Sachs-Teller relations for uniaxial crystals as[42]:

$$\varepsilon_0^{\perp}/\varepsilon_\infty^{\perp} = \prod_i \frac{\omega_{Li}^{\perp}}{\omega_{Ti}^{\perp}} \tag{2}$$

$$\varepsilon_0^{\parallel}/\varepsilon_\infty^{\parallel} = \prod_i \frac{\omega_{Li}^{\parallel}}{\omega_{Ti}^{\parallel}}, \tag{3}$$

where *i* denotes polar mode, $\omega_{Ti}^{\perp}(\omega_{Ti}^{\parallel})$ and $\omega_{Li}^{\perp}(\omega_{Li}^{\parallel})$ are the frequencies of TO and LO components of the E (B)-symmetry modes, respectively. As it seen from the Table 1 we resolved most of E (B) TO/LO peaks and substituting these values to Eqs. (2) and (3) we found experimental ratios of $\varepsilon_0^{\perp}/\varepsilon_\infty^{\perp} \approx 1.14$ and $\varepsilon_0^{\parallel}/\varepsilon_\infty^{\parallel} \approx 1.12$. These results are in good agreement with the values $\varepsilon_0^{\perp}/\varepsilon_\infty^{\perp} \approx 1.12$ and $\varepsilon_0^{\parallel}/\varepsilon_\infty^{\parallel} \approx 1.14$ obtained from the substitution of theoretical phonon frequencies (Table 1, ref. 32). Theoretical values for static dielectric constant $\varepsilon_0^{\perp}$ and $\varepsilon_0^{\parallel}$ are 9.1 and 9.8[4] and high frequency dielectric constants $\varepsilon_\infty^{\perp}$ and $\varepsilon_\infty^{\parallel}$ are 6.8 and 6.6[43], which results in larger ratios $\varepsilon_0^{\perp}/\varepsilon_\infty^{\perp} \approx 1.34$ and $\varepsilon_0^{\parallel}/\varepsilon_\infty^{\parallel} \approx 1.48$ than those determined from phonon frequencies. This found discrepancy is most likely related to some overestimation in calculation of the $\varepsilon_0^{\perp}$ and $\varepsilon_0^{\parallel}$ constants performed in ref. 4, while $\varepsilon_\infty^{\perp}$ and $\varepsilon_\infty^{\parallel}$ values[31] agree well with $\varepsilon_\infty \approx 7$ measured by ellipsometry on CZTS[44].

Conclusions

Summarizing results presented above, from the polarized Raman scattering investigations performed on Cu_2ZnSnS_4 single crystals we experimentally determined the symmetry of 20 from 27 possible modes. The third A symmetry mode frequency was found at 276 cm^{-1}, which was supported by previously published *ab-initio* calculations. The ratio of Raman tensor elements were obtained for most of the observed peaks and a strong difference in *c* and *d* elements of polar B modes and no pronounced difference of *a* and *b* and of *e* and *f* elements of non-polar A and polar E modes was revealed. For the resonant conditions Raman scattering measurements revealed an enhancement in intensity of the polar E and B modes, which under these conditions do not follow the selection rules. In addition, the ratios of the static to high-frequency optic dielectric constants parallel and perpendicular to the ***c***-crystallographic direction were also extracted by using Lyddane-Sachs-Teller relations. The Raman scattering results obtained in the present study could be very useful for the determination of the crystallographic orientations in CZTS semiconductor in bulk and thin film forms.

Experimental details. The CZTS single crystals were grown by chemical vapor transport using iodine as a transporter. The pure elements of Cu, Zn, Sn and S in the stoichiometric proportion were placed in evacuated ampoule together with 5 mg/cm^3 of iodine. The growth process was performed in the vertical two zone furnace during 14 days, and the evaporation and growth temperature were ~800 °C and ~750 °C, respectively. The chemical composition of the bulk single crystals was determined by using X-ray fluorescence. The selected samples were close to stoichiometry (Cu:Zn:Sn:S = 25.3:13.0:11.7:50.0, all values in at.%). The crystal orientation was determined by rotating orientation XRD method, and it revealed that the crystal basal plane is (1 1 2) and the long edge of the crystal platelet is along $[\bar{1}\ 1\ 0]$ direction. All Raman spectra were taken in the backscattering configuration and (**X Y Z**) laboratory coordinate system were used (see Fig. 3). Here **X, Y** and **Z** lie along the $[2\ 2\ 1]$, $[\bar{1}\ 1\ 0]$ and $[\bar{1}\ \bar{1}\ 1]$ crystallographic directions.

Raman spectra were excited by a YAG:Nd solid state laser (line 532 nm) and recorded using a LabRam HR800-UV Horiba Jobin Yvon spectrometer in conjunction with a CCD detector. For the resonant Raman (RR) spectra a solid state laser (line 785 nm) as an excitation source was used. All spectra were measured in backscattering configuration through an Olympus metallographic microscope with convergence power ×50. By using 1800 groove/mm grating and a narrow slit (150 μm), a spectral resolution of ~1 cm^{-1} was achieved. In the measurements the laser power was ~1 mW. At these excitation conditions no thermal effects are observed on the sample surface. Figure 3 shows a schematic representation of the experimental configuration used in these measurements. Note, that polarization of the incident laser beam was fixed and aligned along **Y** axis. The polarization of the scattered beam was changed by using a parallel (gray) and a cross (reddish) polarizer, which were used for the parallel and perpendicular configurations, respectively. In terms of Porto notations[39] the light

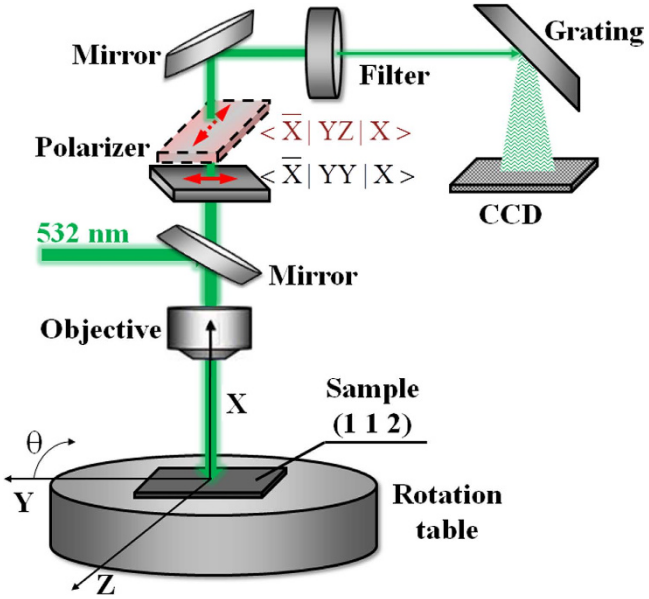

Figure 3. Schematic representation of the experimental configuration used in the polarized Raman experiments performed on the (1 1 2) plane.

propagation in parallel configuration corresponds to the $<\overline{X}|YY|X>$ case, while the cross geometry corresponds to the $<\overline{X}|YZ|X>$ case (Fig. 3). Here the letters outside the line brackets indicate the direction of the incident and scattered light, respectively, while letters inside the line brackets indicate the polarization of the incident and scattered light, respectively[39].

References

1. Wang, W. *et al.* Device Characteristics of CZTSSe Thin-Film Solar Cells with 12.6% Efficiency. *Adv. Energy Mater.* **4,** 1301465 (2014).
2. Zhong, J. *et al.* Sulfurization induced surface constitution and its correlation to the performance of solution-processed $Cu_2ZnSn(S,Se)_4$ solar cells. *Sci. Rep.* **4,** 6288 (2014).
3. Su, C.-Y., Chiu, C.-Y. & Ting, J.-M. Cu_2ZnSnS_4 absorption layers with controlled phase purity. *Sci. Rep.* **5,** 9291 (2015).
4. Paier, J., Asahi, R., Nagoya, A. & Kresse, G. Cu_2ZnSnS_4 as a potential photovoltaic material: A hybrid Hartree-Fock density functional theory study. *Phys. Rev. B* **79,** 115126 (2009).
5. Chen, S. *et al.* Wurtzite-derived polytypes of kesterite and stannite quaternary chalcogenide semiconductors. *Phys. Rev. B* **82,** 195203 (2010).
6. Romero, M. J., Du, H., Teeter, G., Yan, Y. & Al-Jassim, M. M. Comparative study of the luminescence and intrinsic point defects in the kesterite Cu_2ZnSnS_4 and chalcopyrite $Cu(In,Ga)Se_2$ thin films used in photovoltaic applications. *Phys. Rev. B* **84,** 165324 (2011).
7. Bär, M. *et al.* Electronic structure of Cu_2ZnSnS_4 probed by soft x-ray emission and absorption spectroscopy. *Phys. Rev. B* **84,** 035308 (2011).
8. Xu, P. *et al.* Stability and electronic structure of Cu_2ZnSnS_4 surfaces: First-principles study. *Phys. Rev. B* **88,** 045427 (2013).
9. Han, D. *et al.* Deep electron traps and origin of p-type conductivity in the earth-abundant solar-cell material Cu_2ZnSnS_4. *Phys. Rev. B* **87,** 155206 (2013).
10. Leitao, J. P. *et al.* Photoluminescence and electrical study of fluctuating potentials in Cu_2ZnSnS_4-based thin films. *Phys. Rev. B* **84,** 024120 (2011).
11. Chen, S. *et al.* Compositional dependence of structural and electronic properties of $Cu_2ZnSn(S,Se)_4$ alloys for thin film solar cells. *Phys. Rev. B* **83,** 125201 (2011).
12. Paris, M., Choubrac, L., Lafond, A., Guillot-Deudon, C. & Jobic, S. Solid-state NMR and Raman spectroscopy to address the local structure of defects and the tricky issue of the Cu/Zn disorder in Cu-Poor, Zn-Rich CZTS materials. *Inorg. Chem.* **53,** 8646–8653 (2014).
13. Chen, S., Walsh, A., Gong, X.-G. & Wei, S.-H. Classification of lattice defects in the kesterite Cu_2ZnSnS_4 and $Cu_2ZnSnSe_4$ earth-abundant solar cell absorbers. *Adv. Mater.* **25,** 1522–1539 (2013).
14. Levcenko, S., Tezlevan, V. E., Arushanov, E., Schorr, S. & Unold, T. Free-to-bound recombination in near stoichiometric Cu_2ZnSnS_4 single crystals. *Phys. Rev. B* **86,** 045206 (2012).
15. Levcenco, S. *et al.* Influence of anionic substitution on the electrolyt electroreflectance study of band edge transitions in single crystal $Cu_2ZnSn(S_xSe_{1-x})_4$ solid solutions. *Opt. Mater.* **34,** 1362–1365 (2012).
16. Lisunov, K. G. *et al.* Features of the acceptor band and properties of localized carriers from studies of the variable-range hopping conduction in single crystals of p-Cu_2ZnSnS_4. *Sol. Energ. Mater. Sol. Cells* **112,** 127–133 (2013).
17. Guc, M. *et al.* Disorder and variable-range hopping conductivity in Cu_2ZnSnS_4 thin films prepared by flash evaporation and post-thermal treatment. *J. Alloy Compd.* **596,** 140–144 (2014).
18. Grossberg, M., Krustok, J., Raudoja, J. & Raadik, T. The role of structural properties on deep defect states in Cu_2ZnSnS_4 studied by photoluminescence spectroscopy. *Appl. Phys. Lett.* **101,** 102102 (2012).
19. Scragg, J. S., Choubrac, L., Lafond, A., Ericson, T. & Platzer-Björkman, C. A low-temperature order-disorder transition in Cu_2ZnSnS_4 thin films. *Appl. Phys. Lett.* **104,** 041911 (2014).
20. Valakh, M. Y. *et al.* Raman scattering and disorder effect in Cu_2ZnSnS_4. *Phys. Status Solidi (RRL)* **7,** 258–261 (2013).
21. Fontané, X. *et al.* In-depth resolved Raman scattering analysis for the identification of secondary phases: Characterization of Cu_2ZnSnS_4 layers for solar cell applications. *Appl. Phys. Lett.* **98,** 181905 (2011).
22. Fernandes, P. A., Salomé, P. M. P. & Da Cunha, A. F. Study of polycrystalline Cu_2ZnSnS_4 films by Raman scattering. *J. Alloy Compd.* **509,** 7600–7606 (2011).

23. Dimitrievska, M., Fairbrother, A., Pérez-Rodríguez, A., Saucedo, E. & Izquierdo-Roca, V. Raman scattering crystalline assessment of polycrystalline Cu_2ZnSnS_4 thin films for sustainable photovoltaic technologies: Phonon confinement model. *Acta Materialia* **70,** 272–280 (2014).
24. Himmrich, M. & Haeuseler, H. Far infrared studies on stannite and wurtzstannite type compounds. *Spectrochimica Acta* **47A,** 933–942 (1991).
25. Dimitrievska, M. *et al.* Multiwavelength excitation Raman scattering study of polycrystalline kesterite Cu_2ZnSnS_4 thin films. *Appl. Phys. Lett.* **104,** 021901 (2014).
26. Dumcenco, D. & Huang, Y.-S. The vibrational properties study of kesterite Cu_2ZnSnS_4 single crystals by using polarization dependent Raman spectroscopy. *Opt. Mater.* **35,** 419–425 (2013).
27. Rousseau, D. L. Bauman, R. P. & Porto, S. P. S. Normal mode determination in crystals. *J. Raman Spectrosc.* **10,** 253–290 (1981).
28. Guc, M. *et al.* Polarized Raman scattering analysis of $Cu_2ZnSnSe_4$ and $Cu_2ZnGeSe_4$ single crystals. *J. Appl. Phys.* **114,** 193514 (2013).
29. Fontané, X. *et al.* Vibrational properties of stannite and kesterite type compounds: Raman scattering analysis of $Cu_2(Fe,Zn)SnS_4$. *J. Alloy Compd.* **539,** 190–194 (2012).
30. Gurel, T., Sevik, C. & Cagın, T. Characterization of vibrational and mechanical properties of quaternary compounds Cu_2ZnSnS_4 and $Cu_2ZnSnSe_4$ in kesterite and stannite structures. *Phys. Rev. B* **84,** 205201 (2011).
31. Khare, A. *et al.* Calculation of the lattice dynamics and Raman spectra of copper zinc tin chalcogenides and comparison to experiments. *J. Appl. Phys.* **111,** 083707 (2012).
32. Khare, A., Himmetoglu, B., Cococcioni, M. & Aydil, E. S. First principles calculation of the electronic properties and lattice dynamics of $Cu_2ZnSn(S_{1-x}Se_x)_4$. *J. Appl. Phys.* **111,** 123704 (2012).
33. Cardona, M. & Güntherodt, G. *Light Scattering in Solids II* (Springer, 1982).
34. Guc, M. *et al.* Polarized Raman scattering analysis of Cu_2ZnSiS_4 and $Cu_2ZnSiSe_4$ single crystals. *J. Appl. Phys.* **114,** 173507 (2013).
35. Litvinchuk, A. P. *et al.* Electronic structure, optical properties, and lattice dynamics of orthorhombic Cu_2CdGeS_4 and Cu_2CdSiS_4 semiconductors. *Phys. Rev. B* **90,** 165201 (2014).
36. Guc, M. *et al.* Optical phonons in wurtzstannite Cu_2ZnGeS_4 semiconductor: polarized Raman spectroscopy and first principle calculations. *Phys. Rev. B* **89,** 205205 (2014).
37. Valakh, M. Ya. *et al.* Fermi resonance in phonon spectra of quaternary chalcogenides of the type Cu_2ZnGeS_4. *J. Phys.: Condens. Mat.* (accepted).
38. Mai, D. L., Park, H. J. & Choi, I. H. Growth of Cu_2ZnSnS_4 crystals by the directional freezing method with an induction heater. *J. Cryst. Growth* **402,** 104 (2014).
39. Porto, S. P. S. & Krishnan, R. S. Raman Effect of Corundum. *J. Chem. Phys.* **47,** 1009 (1967).
40. Susaki, M. M., Yamamoto, N., Prevot, B. & Schwab, C. Multiple-Phonon Resonant Raman Scattering in $CuGaS_2$. *Jpn. J. Appl. Phys.* **35,** 1652 (1996).
41. Wakita, K., Hirooka, H., Yasuda, S., Fujita, F. & Yamamoto, N. Resonant Raman scattering and luminescence in $CuInS_2$ crystals. *J. Appl. Phys.* **83,** 443 (1998).
42. Cochran, W. & Cowley, R. A. Dielectric constants and lattice vibrations. *J. Phys. Chem. Solids* **23,** 447–450 (1962).
43. Persson, C. Electronic and optical properties of Cu_2ZnSnS_4 and $Cu_2ZnSnSe_4$. *J. Appl. Phys.* **107,** 053710 (2010).
44. Li, J. *et al.* Spectral optical properties of Cu_2ZnSnS_4 thin film between 0.73 and 6.5 eV. *Opt. Express* **20,** A327–A332 (2012).

Acknowledgements

The research leading to these results has received funding from the People Programme (Marie Curie Actions) of the European Union's Seventh Framework Programme FP7/2007-2013/ under REA Grant agreement n°269167 (PVICOKEST) and by MINECO (Ministerio de Economía y Competitividad de España) under the SUNBEAM project (ENE2013-49136-C4-1-R). Authors from the Institute of Applied Physics appreciate the financial supports from STCU 5985 and from the Institutional Project CSSDT 15.817.02.04A. The research was also partially supported by European Regional Development Funds (ERDF, FEDER Programa Competitivitat de Catalunya 2007–2013). Authors from IREC and the University of Barcelona belong to the M-2E (Electronic Materials for Energy) Consolidated Research Group and the XaRMAE Network of Excellence on Materials for Energy of the "Generalitat de Catalunya." V.I.-R. acknowledges the support from MINECO, Subprogram Juan de la Cierva (ref. JCI-2011-10782).

Author Contributions

I.V.B. and L.V.V. grown the single crystals. M.G. and X.F. performed the polarized Raman scattering measurements. V.I.-R. supervised the experimental process and discussed the results. M.G. and S.L. carried out the major part of analysis of experimental data and wrote the paper. E.A. and A.P.-R. supervised the whole work, discussed the results and commented on the manuscript. All authors reviewed the manuscript.

Additional Information

Supplementary information accompanies this paper at http://www.nature.com/srep

Competing financial interests: The authors declare no competing financial interests.

How to cite this article: Guc, M. *et al.* Polarized Raman scattering study of kesterite type Cu_2ZnSnS_4 single crystals. *Sci. Rep.* **6**, 19414; doi: 10.1038/srep19414 (2016).